Synthesis of a nanostructure ion sieve with improved lithium adsorption capacity

Saeed Zandevakili[1], Mohammad Ranjbar[2], Maryam Ehteshamzadeh[3]

[1]*Department of Mining Engineering, Shahid Bahonar University, Kerman, PO Box 76169-133, Iran*
[2]*Mineral Industries Research Centre, Shahid Bahonar University, Kerman, PO Box 76169-133, Iran*
[3]*Department of Material Engineering, Shahid Bahonar University, Kerman, PO Box 76169-133, Iran*
E-mail: saeedzand2001@yahoo.com

Published in Micro & Nano Letters; Received on 16th February 2014; Revised on 1st April 2014; Accepted on 10th June 2014

The low lithium adsorption capacity of different ion sieves was found to be an important limiting parameter for their use in industrial extraction. The maximum exchange capacity of 6.6 mmol/g obtained till now is not high enough for their economical industrial application. Therefore, an increase in lithium adsorption capacity by studying the effects of three parameters, involving manganese salt compound, lithium salt compound and Li/Mn mole ratio on synthesised ion sieves was investigated. Moreover, the ion sieves capability on the lithium uptake from lithium-enriched solution was examined by the Taguchi experimental design method by L9 orthogonal array. Continuously, optimum conditions were predicted and confirmed by the experimental results. Based on the results, all mentioned parameters have significant effect on lithium uptake capacity, but lithium salt compound is the most effective factor. Finally, an appropriate ion sieve with lithium adsorption capacity >8.5 mmol/g was synthesised by applying the optimised conditions.

1. Introduction: The attention given to lithium resources has increased because of its wide application in a variety of industries [1]. The total available lithium in lake brines and several mineral resources is estimated to be about 17×10^6 tons [1]. In the 2012 Mineral Commodity Summaries, the US Geological Survey reported that the USA was a major producer of downstream lithium compounds [2]. According to TRU Group Inc., a world leader in lithium resource evaluation, exploitation and extraction, the demand curve for lithium is expected to increase from about 28 000 tons total global demand in 2012 to about 54 000 tons in 2020 [2, 3]. Therefore alternative resources need to be established to satisfy increasing demand. Seawater is considered as a vast resource of lithium metal (about 2.5×10^{11} tons), with a very low lithium concentration of about 0.17 mg/l [4]. Lithium manganese spinel oxide, expressed by the formula $(Li)_{8a\ Tetrahedral}[Li_xMn_{2-x}]_{16d\ OctaHedral}O_4$, whose oxygen atoms construct the cubic closed-packed framework [5], has been considered to be one of the most promising materials for lithium extraction [6]. Based on this formula, different types of lithium manganese oxides can be considered, because manganese takes both the trivalent and the tetravalent states and the lithium content varies widely [5]. In view of the fact that Mn^{3+} in the spinel will be disproportionate to Mn^{2+}, and Mn^{4+}, and Mn^{2+} dissolves in the acid solution, the investigators attempts have been assigned to increasing Mn^{4+} to preserve spinel skeleton at acidic condition and consequently synthesised some lithium-rich spinel material to overcome this deficiency, such as $Li_{1.33}Mn_{1.67}O_4$ and $Li_{1.6}Mn_{1.6}O_4$ which are formed with only tetravalent manganese [7–9]. Research studies have shown that the Li/Mn mole ratio had significant effects on the ability of Li^+ incorporation from LiOH solutions [7, 10]. However, there have been no systematic studies on the effect of lithium and manganese composition on the synthesised ion sieves and finally Li^+ extraction process. The Taguchi experimental design method is a well-known powerful and efficient tool for multifactor process optimisation, which was used to study a large number of variables with a small number of experiments [11, 12]. Hence, orthogonal arrays were used where each variable setting occurs the same number of times and none of the two experiments are the same [11]. In summary, the main objective of the study reported in this Letter is to optimise the synthesis process of manganese oxide as lithium ion sieves using different constituents, especially manganese and lithium salts. Moreover, the effects of these components and the Li/Mn mole ratio on the lithium adsorption capacity of synthesised ion sieves are investigated.

2. Experimental procedures

2.1. Synthesis of ion sieves: Mn–O nanoparticles were initially prepared through a controlled low-temperature hydrothermal method by oxidation of manganese salt compound with $(NH_4)_2S_2O_8$. Accordingly, a 250 ml mixed solution of manganese salt compound (0.33 mol/l) with $(NH_4)_2S_2O_8$ (0.33 mol/l) was prepared and then transferred into a stainless steel autoclave, sealed, then heated at 120°C for 12 h. Afterwards, the produced black precipitation was filtered, and washed with deionised water to remove extra ions from the final products, and finally dried at 100°C for 12 h in static air to produce a black nanopowder of MnO_2 which is known as (MO). Furthermore, the Li–Mn–O precursor, named (LMO), was prepared by wet impregnation of an aqueous solution of lithium salt compound (0.6 mol/l), with different designed Li/Mn mole ratios with black solid (MO); successively, the mixture was heated in an oven at 100°C for 12 h to remove water and then calcined at 450°C for 6 h in static air. The Li^+ extraction was carried out batchwise by stirring 1.5 g of LMO material with 1 l of a 0.5 M HCl solution for two days. Finally, the acid-treated materials, named (HMO), were filtered, washed with deionised water and dried at 100°C for 12 h to obtain the final ion sieve.

2.2. Design of experiments: Experiments were conducted using the Taguchi experimental design. The Taguchi approach developed rules for carrying out experiments, which further simplify and standardise the experimental design [13]. The permissible range of the input factors and their importance on the design output can be achieved by fully understanding the process. In these experiments, as shown in Table 1, three factors in three levels were taken as variables, which were manganese salt compound (Mn.S.C.), lithium salt compound (Li.S.C.) and Li/Mn mole ratio (Mol.R.).

The Taguchi orthogonal arrays of $L_9(3^4)$ were employed for this study, which can be observed in Table 2. The effect of each control factor at a given level can be estimated using the analysis of the mean and then the optimum levels of control factors for the

Table 1 Main controlling factors and their levels

Factors	Levels		
	1	2	3
(Mn.S.C.)	$MnSO_4{\cdot}H_2O$	$MnCl_2{\cdot}6H_2O$	$Mn(NO_3)_2{\cdot}4H_2O$
(Li.S.C.)	LiOH	$LiNO_3$	$Li_2B_4O_7$
(Mol.R.)	0.6	1	1.5

nanostructure lithium ion sieves with better yield can be obtained [14, 15]. A statistical variance analysis (ANOVA) was performed to determine the effective parameters and their confidence levels. *F*-test is a powerful tool to find out which parameters have significant effects on a defined condition [12]. For this purpose, the *F* value of all factors was compared with the *F* value of the table for α: (risk) = 0.05. If the *F* value of a factor is greater than the *F* value α: (risk), then it means that the variance of the factor is significant compared with the variance of error, and this factor has a significant effect on the response [13, 16]. Then, a verification experiment was performed to verify the optimum parameters [15]. In this work, the lithium uptake was carried out by stirring (300 rpm) 100 mg of each ion sieve in 100 ml of buffer enriched-lithium solution (pH = 11) with a uniform initial Li^+ concentration of 20 mmol/l at 25°C, and the Li^+ concentration in the supernatant solution was determined after 120 h by inductively coupled plasma optical emission spectrometry. Q_e the amount of Li^+ adsorbed per gram of ion sieve at equilibrium (mmol/g) was also calculated according to (1), in which C_e is the concentration of metal ions at equilibrium (mmol/l); C_0 is the initial concentration of lithium ions (mmol/l); W is the weight of adsorbent (g) and V is the solution volume (ml) [8, 17]

$$Q = \frac{(C_0 - C_e)}{W} V \tag{1}$$

2.3. pH titration: A 100 mg of the optimised ion sieve of the confirmation test samples was immersed in a mixed solution containing 10 ml of 0.1 M [MCl + MOH (M: Li, K)] in varying ratios with intermittent shaking at 303 K. After the sample was shaken for five days, the pH of the supernatant solution was determined with a Genway Model 3540pH meter.

2.4. Materials characterisation: The crystalline structure of the precursor and synthesised adsorbent were determined by X-ray phase analysis (XRD, PHILIPS, X'pert MPD system, $\lambda = 1.54$ Å) with Kα Cu radiation. The morphology and average particle size of the synthesised adsorbent nanoparticles were characterised by scanning electron microscopy (SEM, Tescan Vega-II) and transmission electron microscopy (TEM, PHILIPS CM20). The inductively coupled plasma optical emission spectrometry (ICP, VARIAN OES) was used for the determination of initial and final Li^+ concentrations. Infrared (IR) spectra were recorded on a Bruker tensor 27 FTIR spectrometer with an RT-DLATGS detector, in the range of 400–4000 cm^{-1} with a spectral resolution of 4 cm^{-1} in transmittance mode. The KBr pellet technique was used for sample preparation with about 1 wt% of sample.

Table 2 Experimental condition based on Taguchi $L_9(3^4)$ standard orthogonal array and results

Exp.no.	(Mn.S.C.)	(Li.S.C.)	(Mol.R.)	Adsorption, mmol/g
1	$MnSO_4{\cdot}H_2O$	LiOH	0.6	5.89
2	$MnSO_4{\cdot}H_2O$	$LiNO_3$	1	7.44
3	$MnSO_4{\cdot}H_2O$	$Li_2B_4O_7$	1.5	2.33
4	$MnCl_2{\cdot}6H_2O$	LiOH	1	1.96
5	$MnCl_2{\cdot}6H_2O$	$LiNO_3$	1.5	3.24
6	$MnCl_2{\cdot}6H_2O$	$Li_2B_4O_7$	0.6	1.47
7	$Mn(NO_3)_2{\cdot}4H_2O$	LiOH	1.5	3.56
8	$Mn(NO_3)_2{\cdot}4H_2O$	$LiNO_3$	0.6	8.49
9	$Mn(NO_3)_2{\cdot}4H_2O$	$Li_2B_4O_7$	1	2.4

Table 3 Analysis of variance $F(0.05, 2, 2) = 19$

	SS_{factor}	d_f	V	F_{value}	P_{value}	P%
model	51.9	6	8.65	61.24	0.0162	
(Mn.S.C.)	15.87	2	7.93	56.18	0.0175	30.41
(Li.S.C.)	28.4	2	14.2	100.54	0.0098	54.42
(Mol.R.)	7.63	2	3.82	27.02	0.0357	14.062
error	0.28	2	0.14			0.55
total	52.18	8				

3. Results and discussion

3.1. Design of experiment: The whole lithium uptake with synthesised ion sieves is also listed in Table 2. The lithium adsorption capacity ranges from 1.47 to 8.49 mmol/g. Table 3 shows the results of the analysis of variance (ANOVA). In this Table, the sum of squares (SS_{Factor}), degrees of freedom (d_f) and the mean of squares ($V = SS_{Factor}/d_f$) are represented, respectively. Subsequently, the *F*-value ($F_{factor} = V_{factor}/V_{error}$), *P*-value and percentage of contribution for each factor ($P\% = SS_{factor}/SS_{total}) \times 100$ were calculated. As illustrated in Table 3, the *F*-value of the whole factors was greater than the extracted *F*-value of the table for $\alpha = 0.05$. It means that the variance of all factors is significant compared with the variance of error and all of them have a significant effect on the response. The significance of each coefficient was also determined by *P*-values, which are listed in Table 3. *P*-values <0.05 indicate that the model terms are significant. Consequently, the results of *F*-value and *P*-value confirm each other. Finally, the contribution of each factor to the synthesised ion sieves for lithium adsorption was determined as presented in Table 3. This analysis reveals that the order of factors influences the lithium uptake is Li.S.C. > Mn.S.C. > Mol. R., respectively. The error variance contribution is 0.54%. In other words, the experiment in this work has 99.4% of confidence if the interaction of factors is not considered.

Fig. 1 shows the effect of each parameter level on the response variable and demonstrates that the best adsorption obtained when Mn.S.C. was set at the first and the third, Li.S.C. at the second and Mol.R. at the first levels. Moreover, factor Li.S.C. is the most significant factor, because of the fabrication of the strong acidity sites during the synthesis process. Generally, in equilibrium reaction $R-H^+ + Li^+ \Leftrightarrow R-Li^+ + H^+$ according to the Le Chatelier's principle, increasing the lithium uptake could be achieved by removing proton ions from the medium solution, which could be

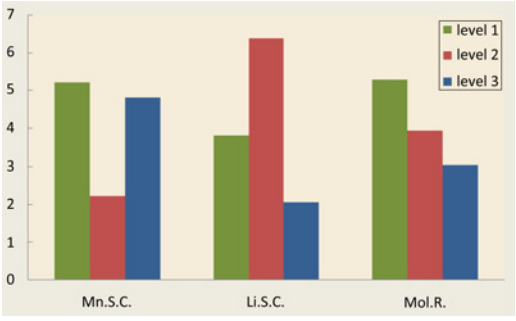

Figure 1 *Effect of each parameter level on the response variable*

doi: 10.1049/mnl.2014.0086

attained by adding OH^- ions. Increasing the solution's pH or enhancing the intrinsic acidity of the exchange sites increases lithium ion adsorption. It seems that the increase in intrinsic acidity of the ion sieve sites could be assigned to the nucleating pH during processing. Therefore strong acidity is advantageous for the sorption of lithium from a weakly basic solution like seawater [5, 18] and the large lithium uptake of the present samples in experiments number 8 and 2 are due to the availability of strongly acidic sites in the ion sieve. Consequently, pH titration is used after identifying the optimum condition of variables and performing the confirmation tests. Regarding the Mn.S.C. factor, uptake of lithium ions increases in the order of $MnCl_2{\cdot}6H_2O < Mn(NO_3)_2{\cdot}4H_2O < MnSO_4{\cdot}H_2O$. Concerning the Li.S.C. factor, increase in lithium adsorption follows the order of $Li_2B_4O_7 < LiOH < LiNO_3$. Furthermore, the effect of factor Mol.R. is shown in Fig. 1. As can be seen, increase in Mol.R. decreases the lithium uptake. This could be satisfied by the generation of different amounts of impurity phases such as Mn_2O_3 and Mn_3O_4, in addition to the pure spinel phase, especially when Mol.R. is >0.7. This fact is confirmed in [7]. Prediction of lithium uptake at optimised conditions was the last objective of the Taguchi statistical design and one of the most important goals of this research. Whenever the optimum condition of the factors and levels are identified, an optimised lithium ion sieve will be predicted by (2) and (3) [19, 20]

$$Y_{\text{Opt}} = \bar{y} + (A_1 - \bar{y}) + (B_2 - \bar{y}) + (C_1 - \bar{y}) = 8.7 \quad (2)$$

$$\overline{Y} = \frac{\sum_{i=1}^{n} y_i}{n} = 4.086 \quad (3)$$

In (2), Y_{Opt} is the predicted surface area at the optimum condition and in (3)$\bar{y}$ is the grand average of the responses. After prediction, a confirmation test should be conducted. In this step, two samples were prepared under optimum condition (Mn.S.$C_{1\ \text{and}\ 3}$, Li.S.C_2 and Mol.R_1) named samples 10, 11. The lithium uptake of samples 10 and 11 was measured as 8.04 and 8.56 mmol/g, respectively. The best result formed under optimum condition (Mn.S.C_3, Li.S.C_2 and Mol.R_1) and the difference between the predicted (8.7 mmol/g) and the achieved values is negligible and the low error of (1.6%) confirms the predictability of the process and accuracy of the experimental results.

3.2. pH titration: The pH titration curves of ion sieve samples from confirmation tests in (0.1 M LiCl + LiOH) and (0.1 M KCl + KOH) solutions are shown in Fig. 2. The apparent capacities for Li^+ were remarkably larger than those for K^+ over the pH range studied, indicating that both the samples showed lithium ion sieve properties. The high selectivity for Li^+ is due to the specific effect of the insertion site. The K^+ ion uptake can be regarded as the number of non-specific sites on the surfaces of the powder. Therefore it can be concluded that sample 11 characteristically

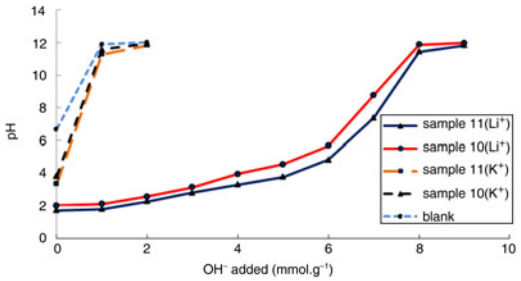

Figure 2 *pH titration curve of ion sieve samples from confirmation tests towards lithium and potassium ions*
Solution, 0.1 M [MCl + MOH (M: Li, K)] $T = 303$ K, $V = 0$ ml, $W = 100$ mg, time = 5 days

Table 4 Comparison of lithium uptake by different ion sieves and the synthesised ion sieve in this study

Li^+ uptake, mmol/g	References	Li^+ uptake, mmol/g	References
0.014	[21]	5.38	[25]
2	[22]	3.42	[26]
3.6	[4]	5.57	[9]
5.3	[4]	1.53	[8]
3.8	[23]	2.91	[8]
3.17	[7]	1.35	[8]
2.4	[24]	6.67	[18]
6.62	[17]	8.56	new sieve
5.33	[1]		

has large numbers of uniform sorption sites with relatively strong acidity compared with the other sample. As mentioned before, the large lithium uptake of sample 11 is due to the availability of strong acidic sites inside the solid. However, the effects of other effective factors such as crystal structure, morphology, size and accompanying impurities of the ion sieve should not be overlooked.

According to the literature [1, 4, 7–9, 17, 18, 21–26], the Li^+ adsorption capacity of different synthesised ion sieves from liquid lithium-enriched resources are as listed in Table 4. As shown in this Table, the maximum uptake capacity of previous lithium ion sieves does not exceed 6.67 mmol/g. Meanwhile, by the optimisation of variables involved in the synthesis process, the ability to synthesise a lithium ion sieve with an adsorption capacity >8.5 mmol/g has been provided for the first time. Therefore this material can be economically justified to extract lithium from liquid resources and has a less polluting effect on the environment. Moreover, the present ion sieve is the most promising adsorbent of lithium in seawater.

3.3. IR result: As shown in Fig. 3, IR spectroscopic analysis was carried out on the precursor and ion sieve samples, resulting from the optimised condition. In the spectra of the precursor sample, the absorption band at 3425 cm^{-1} and bands at 1631 cm^{-1} can be assigned to stretching and bending vibrations of water [27]. The bands in the region of 400–700 cm^{-1} can be assigned to Mn–O stretching vibrations [27, 28] and depending on the Mn–O vibrations are changed slightly by the extraction of lithium ions [27]. A new band at 910 cm^{-1} and a shifted band at 3349 cm^{-1} appeared after the extraction of Li^+ by the ion sieve systems. The

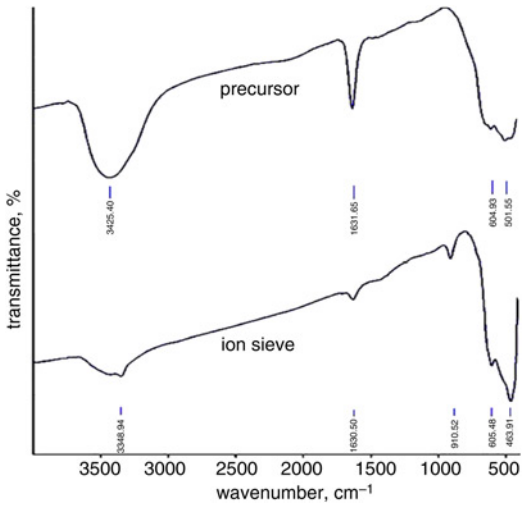

Figure 3 *IR spectra of precursor and ion sieve*

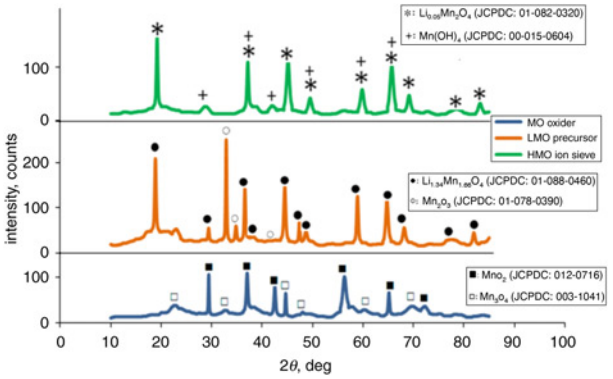

Figure 4 *XRD patterns of various manganese oxides*

band at 3349 cm^{-1} can be assigned to the stretching vibration of the lattice –OH group, and the band at 910 cm^{-1} to lattice coupling vibration of the H^+ form spinel. These results correlate well with the fact that the Li^+/Mn^+ reaction occurs in the systems and protons get into the spinel structure and form the hydroxyl groups with oxygen in the lattice [1, 27].

3.4. XRD results: Phase analyses of manganese oxide (MO), lithium manganese precursor as ternary oxide (LMO) and delithiated lithium manganese spinel powders (HMO) are given in Fig. 4. The reflections of (MO) strong peaks can be readily indexed to pyrolusite MnO_2 phase [space group: P42/mnm (136), JCPDS 12-0716]. The weaker peaks related to Mn_3O_4 as impurity within the main phase of pyrolusiteMnO_2. The (LMO) sample showed $Li_{1.34}Mn_{1.66}O_4$ crystallisation [space group: Fd3 m (227), JCPDS 1-088-0460] with lattice constant $a = 8.1407$ Å. This resulted from the fact that some Li atoms replace the Mn atoms in the octahedral sites (16d) inducing the increase of the Mn chemical state from 3.5^+ to 4^+ and stronger chemical bonding of Mn^{4+}–O^{2-} [17]. The more compact the Mn–O lattices the more stable the $Li_{1.34}Mn_{1.66}O_4$ spinel after the Li^+ extraction [17, 18]. Moreover, the presence of two peaks between 30° and 40° verifies the existence of the Mn_2O_3 phase [space group: Ia-3 (206), JCPDS 1-078-0390] next to $Li_{1.34}Mn_{1.66}O_4$. The (HMO) ion sieve could be indexed to the cubic phase $Li_{0.05}Mn_2O_4$ [space group: Fd3 m (227), JCPDS 1-082-0320] with lattice constant $a = 8.0445$ Å, calculated according to the Bragg formula [17]. Consequently, most of the lithium ions of the precursor exited from the spinel structure which must be replaced by proton ions.

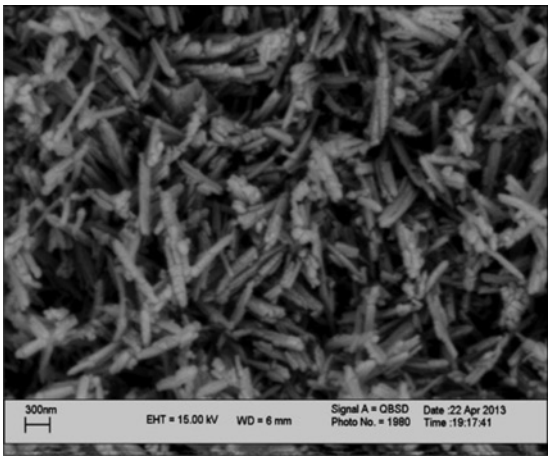

Figure 5 *SEM image of MnO_2 ion sieve*

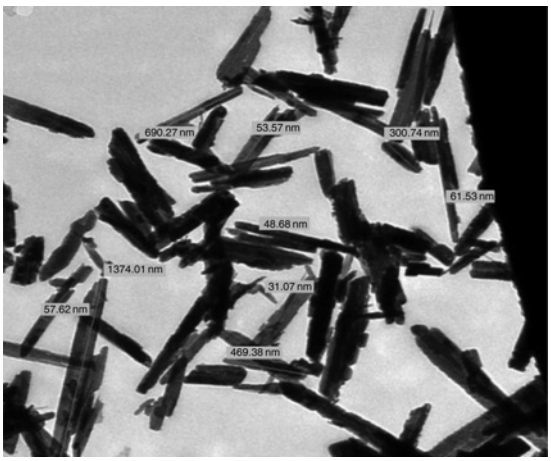

Figure 6 *TEM image of MnO_2 ion sieve*

This fact is confirmed by IR results. Hence, the (HMO) ion sieve can be summarised as $MnO_2{\cdot}xH_2O$. Moreover, the presence of $Mn(OH)_4$ besides the $Li_{0.05}Mn_2O_4$, confirms the formation of the hydroxyl group. The crystallisation of the delithiated powders (ion sieves) were the same as the precursor, but the peaks shifted to higher 2θ values. This phenomenon was discussed by Wang (2009) that during delithiation process the original spinel structure was preserved by increasing the crystalline size. According to Bragg's law ($n\lambda - 2d\sin\theta$), the shifting of the peaks to higher 2θ values should be related to the decrease in the distance between planes (d) during the delithiation process in which the small ion (H^+) takes the position of the large ion (Li^+) [9, 29].

3.5. SEM and TEM results: The SEM result of the MnO_2 ion sieve is presented in Fig. 5. The prepared powder shows a nanorod morphology with bulky aggregates. The formation mechanism of the agglomerated particles was cleared by evaporation and decomposition reactions of the aerosol droplets obtained from clear solutions [9].

The TEM image of the HMO sample presented in Fig. 6 illustrates nanorods with an average size of about 50 nm in diameter and 800 nm in length, while the average particle ion sieves size of 100×2500 nm^2 was reported by previous studies [17]. A smaller size provides a bigger surface area and enhances the adsorption of Li^+ions [12]. The high uptake rate and capacity can be related to the special particle structure of the ion sieve (porous structure), with smaller size especially in length. Thus, the lithium can enter the pores from medium solution and cover the nanorod particles and because of the ion sieve special structure the pathway between Li^+ and H^+ ns during the ion exchange process becomes shorter. Therefore the ion exchange process can be performed easily.

4. Conclusion: In this reported study, a nanostructured lithium ion sieve was synthesised via the hydrothermal process. The effects of the three parameters including: Mn.S.C., Li.S.C. and Mol.R., in three levels on lithium adsorption capacity of synthesised ion sieves were investigated using the Taguchi experimental design method [by $L_9(3^4)$orthogonal array]. ANOVA analysis was applied to evaluate the relative importance of the effects of various factors. From the results of this study, it can be concluded that the Li.S.C. had the most significant effect on lithium adsorption. Maximum lithium uptake was achieved using the synthesised ion sieve, formed with the combination of Mn $(NO_3)_2{\cdot}4H_2O$, $LiNO_3$ and Li/Mn mole ratio equal to 0.6. For the first time a lithium ion sieve with an adsorption capacity >8.5 mmol/g was synthesised.

doi: 10.1049/mnl.2014.0086

5 References

[1] Wang L., Meng C., Ma W.: 'Preparation of lithium ion-sieve and utilizing in recovery of lithium from seawater', *Front. Chem. Eng. China*, 2009, **3**, (1), pp. 65–67

[2] Amerilithium: 'Corporate presentation', 2012. Available at http://www.amerilithium.com/AMEL_Presentation_Q3_2012.pdf

[3] TRU-Group.: 'Lithium Pipeline Projects cannot beat the Existing Lithium Chemical Big Three', 2011. Available at http://trugroup.com/whitepapers/TRU-Lithium-Press-Release-2011-01-17.pdf

[4] Chitrakar R., Kanoh H., Miyai Y., Ooi K.: 'Recovery of lithium from seawater using manganese oxide adsorbent ($H_{1.6}Mn_{1.6}O_4$) derived from $Li_{1.6}Mn_{1.6}O_4$', *Ind. Eng. Chem. Res.*, 2001, **40**, (9), pp. 2054–2058

[5] Chitrakar R., Kanoh H., Miyai Y., Ooi K.: 'A new type of manganese oxide ($MnO_2{\cdot}0.5H_2O$) derived from $Li_{1.6}Mn_{1.6}O_4$ and its lithium ion-sieve properties', *Chem. Mater.*, 2000, **12**, (10), pp. 3151–3157

[6] Piszora P., Paszkowicz W., Baehtz C., Wolska E.: 'X-ray diffraction studies on the nature of the phase transition in the stoichiometric $LiMn_2O_4$', *J. Alloys Compd.*, 2004, **382**, (1–2), pp. 119–122

[7] Wang L., Ma W., Liu R., Li H.Y., Meng C.G.: 'Correlation between Li^+ adsorption capacity and the preparation conditions of spinel lithium manganese precursor', *Solid State Ion.*, 2006, **177**, (17–18), pp. 1421–148

[8] Ma L.W., Chen B.Z., Shi X.C., Zhang W., Zhang K.: 'Stability and Li^+ extraction/adsorption properties of $LiM_xMn_{2-x}O_4$ in aqueous solution', *Colloid Surf. A*, 2010, **369**, (1–3), pp. 88–94

[9] Özgür C.: 'Preparation and characterization of $LiMn_2O_4$ ion-sieve with high Li^+ adsorption rate by ultrasonic spray pyrolysis', *Solid State Ion.*, 2010, **181**, (31–32), pp. 1425–1428

[10] Wang L., Meng C.G., Ma W.: 'Study on Li^+ uptake by lithium ion-sieve via the pH technique', *Colloid Surf. A*, 2009, **334**, (1–3), pp. 34–39

[11] Taguchi G., Yokoyama Y.: 'Taguchi methods: design of experiments' (ASI Press, 1993)

[12] Tofighy M.A., Mohammadi T.: 'Salty water desalination using carbon nanotube sheets', *Desalination*, 2010, **258**, (1), pp. 182–186

[13] Sadrzadeh M., Mohammadi T.: 'Sea water desalination using electrodialysis', *Desalination*, 2008, **221**, (1–3), pp. 440–447

[14] Chou C.S., Yang R.Y., Chen J.H., Chou S.W.: 'The optimum conditions for preparing the lead-free piezoelectric ceramic of $Bi_{0.5}Na_{0.5}TiO_3$ using the Taguchi method', *Powder Technol.*, 2010, **199**, (3), pp. 264–271

[15] Liu W.L., Hsieh S.H., Chen W.J., Lee J.H.: 'Study of nanosized zinc oxide on Cu–Zn alloy substrate using Taguchi method', *Surf. Coat. Technol.*, 2007, **201**, (22–23), pp. 9238–9242

[16] Mohammadi T., Moheb A., Sadrzadeh M., Razmi A.: 'Separation of copper ions by electrodialysis using Taguchi experimental design', *Desalination*, 2004, **169**, (1), pp. 21–31

[17] Zhang Q.H., Li Sh.P., Sun S.Y., Yin X.S., Yu J.G.: 'Lithium selective adsorption on 1-D MnO2 nanostructure ion-sieve', *Adv. Powder Technol.*, 2009, **20**, (5), pp. 432–437

[18] Sun S.Y., Song X., Zhang Q.H., Wang J., Yu J.G.: 'Lithium extraction/insertion process on cubic Li-Mn-O precursors with different Li/Mn ratio and morphology', *Adsorption*, 2011, **17**, (5), pp. 881–887

[19] Roy R.K.: 'Design of experiments using the Taguchi approach: 16 steps to product and process improvement' (Wiley-Interscience, 2001)

[20] Norouzbeigi R., Edrissi M.: 'Modification and optimization of nanocrystalline Al_2O_3 combustion synthesis using Taguchi L16 array', *Mater. Res. Bull.*, 2011, **46**, (10), pp. 1615–1624

[21] Kaneko S., Takahashi W.: 'Adsorption of lithium in sea water on alumina–magnesia mixed-oxide gels', *Colloids Surf.*, 1990, **7**, pp. 69–79

[22] Chitrakar R., Kanoh H., Makita Y., Miyai Y., Ooi K.: 'Synthesis of spinel-type lithium antimony manganese oxides and their Li extraction/ion insertion reactions', *J. Mater. Chem.*, 2000, **10**, (10), pp. 2325–2329

[23] Heng L.J., Xi C.Y., Xia G.Q., Bin S.Y., Jun Z., Hua Y.Q.: 'Preparation of λ-MnO_2 by column method and its ion-sieve property', *J. Wuhan Univ. Technol. Mater. Sci. Ed.*, 2002, **17**, (4), pp. 9–12

[24] Zhang Q.H., Sun S., Li S., Jiang H., Yu J.G.: 'Adsorption of lithium ions on novel nanocrystal MnO_2', *Chem. Eng. Sci.*, 2007, **62**, (18–20), pp. 4869–4874

[25] Tian L., Ma W., Han M.: 'Adsorption behavior of Li^+ onto nano-lithium ion sieve from hybrid magnesium/lithium manganese oxide', *Chem. Eng. J.*, 2010, **156**, (1), pp. 134–140

[26] Zhang Q.H., Li Sh.P., Sun S.Y., Yin X.S., Yu J.G.: '$LiMn_2O_4$ spinel direct synthesis and lithium ion selective adsorption', *Chem. Eng. Sci.*, 2010, **65**, (1), pp. 169–173

[27] Feng Q., Miyai Y., Kanoh H., Ooi K.: 'Lithium(1 +) extraction/insertion with spinel-type lithium manganese oxides. Characterization of redox-type and ion-exchange-type sites', *Langmuir*, 1992, **8**, (7), pp. 1861–1867

[28] Shen X.M., Clearfield A.: 'Phase transitions and ion exchange behavior of electrolytically prepared manganese dioxide', *J. Solid State Chem.*, 1986, **64**, (3), pp. 270–282

[29] Kameshima Y., Yoshizawa A., Nakajima A., Okada K.: 'Solid acidities of SiO_2–TiO_2/montmorillonite composites synthesized under different pH conditions', *Appl. Clay Sci.*, 2009, **46**, (2), pp. 181–184